MSDE

PAPER

View Article Online
View Journal | View Issue

Cite this: *Mol. Syst. Des. Eng.*, 2024, 9, 300

Simultaneous optimisation of shape and magnetisation of nanoparticles synthesised using a green bioinspired route†

Laura Norfolk,[a] Luc Dewulf,[b] Mauro Chiacchia,[b] Siddharth V. Patwardhan *[b] and Sarah S. Staniland ‡*[a]

The bioinspired co-precipitation of magnetite nanoparticles (MNP) using additives to tailor particle shape is an attractive alternative to the currently favoured environmentally unsustainable methods of producing shape-controlled particles. In particular, ethylenediamine based additives are able to produce MNP with high-yield under environmentally friendly conditions, yet with the desired control over particle attributes. The effect of tetraethylenepentamine (TEPA) as an additive in the room-temperature co-precipitation (RTCP) of magnetite has been investigated in an iterative Design of Experiments (DoE) strategy, utilising Full Factorial Designs (FFD) and a Path of Steepest Ascent (PSA) optimisation through three consecutive designs. Considering the ferric ratio (Fe^{3+}/Fe^{2+}), Fe/additive ratio, and timepoint of additive addition as factors, the percentage of isotropic faceted particles and saturation magnetisation were measured as responses. After an initial scouting FFD, timepoint of additive addition was found to be insignificant as a factor. A second FFD followed by a PSA optimisation found higher Fe^{3+}/Fe^{2+} ratios of 0.6, closer to the ideal 2 : 1 stoichiometric ferric ratio produced a higher shape response (an increase in isotropic faceted particles). The interaction between ferric and Fe/additive ratio was found to be significant, as the same level of additive concentration was not as effective at lower ferric ratios. An optimum Fe/additive ratio of 50 : 1 was established, alongside the higher ferric ratio of 0.6 to produce ~90% isotropic faceted particles with a high magnetism of 77 emu g^{-1}, showing it is possible to synthesise MNP which are both highly magnetic and highly faceted. Since it is a requirement of many industries to use homogeneous particles, the predictive synthesis of these magnetite nanoparticles is a significant step towards the industrial production of green magnetite nanoparticles. These conditions can be utilised for further synthesis or as a basis for further optimisation of shape-tuned magnetite nanoparticle syntheses. This DoE strategy enabled the optimisation of two responses simultaneously to produce high quality MNP.

Received 19th October 2023,
Accepted 18th December 2023

DOI: 10.1039/d3me00164d

rsc.li/molecular-engineering

Design, System, Application

A rational design strategy is demonstrated for the room-temperature synthesis of high-quality magnetite nanoparticles (MNP). Specifically, an innovative iterative Design of Experiments (DoE) strategy, utilising Full Factorial Designs (FFD) and a Path of Steepest Ascent (PSA) strategy through three consecutive designs were used. Extensive experimentation, modelling and analysis has led to an optimum set of synthesis parameters which produced ~90% isotropic faceted particles with a high magnetism. The outcomes show a compelling step on the pathway to statistically guided and tunable MNP synthesis, with the shape control of MNP using a green synthesis not yet being extensively researched. By building upon the prior studies, we have furthered our understanding of how synthesis conditions influence the properties of MNP and identified a potential starting point for batch scale-up of isotropic faceted MNP. Further, the results clearly demonstrate the use of our DoE strategy in optimising multiple criteria simultaneously. Specifically, this work shows that it is possible to synthesise MNP which are both highly magnetic and highly faceted. Since it is a requirement of many industries to use homogeneous particles, this predictive synthesis of green nanoparticles is widely applicable to other chemistries and is a significant step towards the industrial production of wider green nanoparticles.

[a] *Department of Chemistry, The University of Sheffield, Dainton Building, Brook Hill, Sheffield, S3 7HF, UK. E-mail: Sarah.Staniland@beis.gov.uk*
[b] *Department of Chemical and Biological Engineering, The University of Sheffield, Mappin Street, Sheffield, S1 3JD, UK. E-mail: s.patwardhan@sheffield.ac.uk*
† Electronic supplementary information (ESI) available. See DOI: https://doi.org/10.1039/d3me00164d
‡ Present address: Government Office for Technology Transfer.

Introduction

For several decades, tailored magnetite nanoparticles (MNP) have been extensively studied[1] for their applications in various industries spanning data storage,[2] ferrofluids for electronics,[3,4] and crucially several biomedical applications

including hyperthermic cancer treatments,[5] targeted drug delivery,[6] and MRI contrast agents.[7] In these applications, particle properties such as size,[8] composition,[9] and shape[10] each play a pivotal role in the performance. As such, it is crucial to be able to modulate these properties in a nanomaterial product. The ability to design and tailor bespoke magnetic nanoparticles controlling these properties has hence been a research goal.

The shape of MNPs has been observed to influence the properties of particles for clinical applications. Octahedral MNPs were found to exhibit higher specific absorption rates and improved relaxivity for MRI use, showcasing the potential advantages of specific morphologies for medical applications.[11]

As industrial use of MNPs rise, it is increasingly clear that producing tailored nanomaterials in a sustainable manner is a critical issue to address.[12] Whilst highly shape-controlled MNPs have been synthesised, the methodologies require high boiling point organic solvents, toxic precursors, and extensive heating and vacuum use,[13,14] rendering them highly unsustainable. On the other hand, achieving enhanced morphological control of MNPs under milder reaction conditions such as a room temperature co-precipitation (RTCP) has proved to be a challenge under laboratory conditions.[15]

As a nanocrystal nucleates and grows from a spherical primary particle, additives such as proteins[16,17] or smaller compounds[18] may interact with the forming magnetite surface. Adsorption of an additive to a crystal face lowers the interfacial energy of that facet, and crystal growth along that axis is slowed, ensuring that this face dominates the final particle morphology.

Research into magnetotactic bacteria,[19] and subsequently their biomineralisation proteins[20,21] and derivatives such as magnetite interacting Adhirons (MIA)[22] has furthered our understanding of how highly faceted magnetite forms in nature under ambient conditions. Drawing inspiration from MIA, the use of small molecular additives incorporating amine functionalities have been found to modulate the shape of MNPs.[23] Ethylenediamine homologues have successfully been used to produce octahedral particles in both batch and large-scale flow co-precipitation reactions, with tetraethylenepentamine (TEPA) being the most successful of this series.[23] Further investigation into the impact and function of TEPA as an additive is important to build on the understanding of how the morphology of MNPs are affected by the addition of TEPA to RTCP reactions, which can help design MNPs for desired applications. Indeed, recently the importance of optimising multiple nanoparticle attributes was emphasised though discovery and design stages[24] and hence this study aims to simultaneously optimise the shape and magnetisation of nanoparticles synthesised using a green bioinspired route.

Previous studies aiming to understand the factor-response relationship of MNPs were often carried out utilising a variation of the one-factor-at-a-time (OFAT) approach. However, univariate methods are unsuited to understand the complex nature of MNP synthesis, and for optimisation of multiple responses such as shape and magnetism simultaneously. Instead, multivariate methods such as those within the Design of Experiments (DoE) framework allow product and process optimisation *via* statistical evidence. The DoE methodology provides efficient designs that designate a combination (treatment) of reaction synthesis parameters (factors) and their physical values (factor levels) according to which experimental results (observations) are collected and statistically analysed.

Generally, designs fall into several categories, two of which will be discussed in this paper: 1) Screening designs are used to segregate significant from insignificant factors and for obtaining preliminary indication of the direction of response improvement, while lacking precision due to their design simplicity. 2) Optimisation frequently employs more elaborate models to obtain an increasingly precise map of the behaviour of the chemical system, at the cost of being more resource intensive. Greater experimental efficiency can be obtained with a combination of these two approaches as we recently successfully demonstrated elsewhere.[25]

For MNPs both screening and optimisation designs have previously been used to gain a better understanding of the input–output relationship between synthesis factors and physicochemical properties. For screening, 2^3 and 2^4 full factorial designs (FFD) were employed to evaluate nanoparticle size, magnetite yield, and magnetisation for electrochemical-, microwave-, and Mössbauer-synthesised magnetite.[26–29] Magnetite *via* co-precipitation was screened using Plackett–Burman and uniform 2^6 fractional factorial designs.[30,31]

A range of optimisation studies have been conducted including central composite designs, Box–Behnken designs, and optimal designs to map particle size, yield, and magnetisation for hydrothermal and co-precipitation magnetite syntheses.[32–37] However, previous studies reveal several drawbacks: all studies performed a single standalone design and did not optimise the system beyond their one-off experiment, with the exception of Medinger *et al.*,[37] who used a feedback loop to refine the response surface methodology. Moreover, studies attempted to optimise only a single response at a time. Instead, we report a sequential strategy consisting of two factorial screening designs, followed by a path of steepest ascent (PSA) optimisation (Fig. 1).

The factorial screening design allows construction of simple polynomial regression models at low experimental cost. The maximum (or minimum) response can be assumed to be in the direction in which the regression model increases (or decreases), although the optimum point may lie outside of the initial screening design space. The path of steepest ascent (or descent) can then be calculated and experiments carried out at regular intervals to locate the maximum (or minimum) response. PSA optimisation is reported for biological[38–43] and organic synthesis,[44,45] but has rarely been employed for inorganic synthesis,[46,47] and is entirely unreported for magnetite synthesis.

In the synthesis of MNP, multiple input parameters affect the output product properties (responses) to various extents,

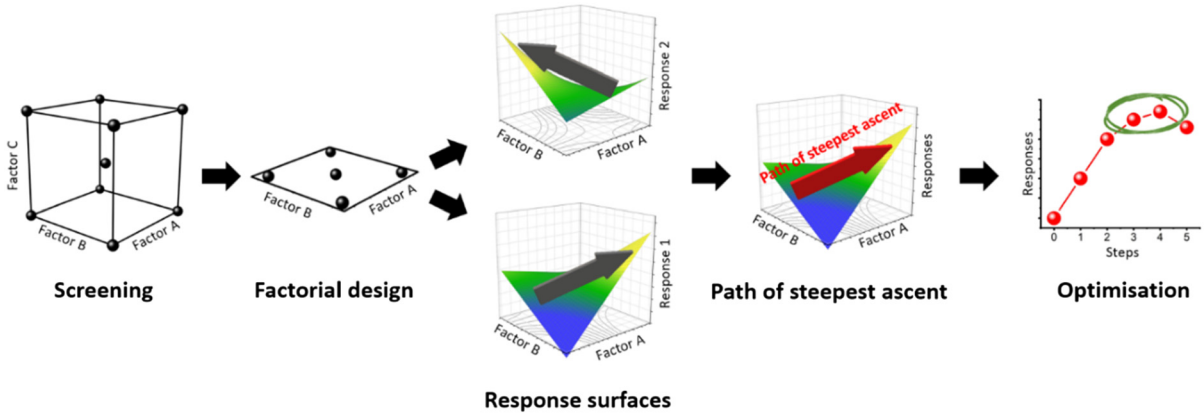

Fig. 1 Sequential Design of Experiments strategy consisting of a factorial screening design followed by a path of steepest ascent to optimise two responses simultaneously.

resulting in an inherently complex reaction landscape. Future scale-up and optimisation depend on the ability to identify the significant from the insignificant factors and to map how the response changes with a change in the identified significant factors.

Previous research has shown the importance of the Fe^{3+}/Fe^{2+} ratio on the size and composition of MNPs formed under RTCP conditions. Particles formed at lower ratios are typically larger in size, with higher polydispersity and a lower proportion of magnetite. Biomineralisation proteins have shown the ability to influence ferrous iron, promoting the formation of magnetite in ferrous-rich environments which would usually be unfavourable for the formation of this desired iron oxide, inspiring the investigation into the potential for additives to alter the proportion of magnetite formed at lower ferric ratios. Varying the ratio from the established ideal of 0.6 allows for the effect of the additive across a spectrum of conditions to be investigated.

pH titrations of the reaction system have identified the time points at which the RTCP is significantly chemically distinct, leading to the selection of three distinct timepoints; t_1, the start of the reaction, t_2, after all soluble iron(III) is consumed, and t_3, after all soluble iron(II) is consumed. The equivalence points at which the ferric/ferrous ions were consumed were taken from Rawlings *et al.* and were determined based on the ferric ratio for each reaction.[16]

Our previous study suggested the ideal Fe/additive ratio to be around 125.[23] Performing reactions above and below this tested value allows the influence of additive concentration to be screened across a range. We are seeking to further improve upon the previously identified optimal conditions and investigate a wider range of concentrations than those previously studied.

Both magnetism and particle shape play an important role in the potency of MNPs as a potential biomedical treatment, and as such both these responses are measured, and optimised using further iterations of DoE.

A total of three iterations of DoE were completed, with two factorial designs, the first of which covering all three factors, the second considering ferric ratio and additive : iron ratio, and finally a path of steepest ascent compromising between optimising both magnetism and the proportion of faceted particles formed.

The complete study of three iterative designs is the first account of systematic optimisation of additive controlled bioinspired magnetite nanoparticle synthesis using a sequential statistical strategy.

Materials and methods

Chemicals

Iron(II) sulphate, iron(III) sulphate, sodium hydroxide and tetraethylenepentamine were purchased from Sigma-Aldrich and used without further purification. Iron contents of the iron salts were assessed *via* inductively coupled plasma optical emission spectrometry analysis when calculating iron solution molarities. Ultrapure water (Milli-Q) (Merck, Milli-Q integral purification system) was used for all experiments.

Magnetite nanoparticle synthesis

To favour the formation of magnetite nanoparticles, all reactions were carried out under an inert atmosphere of N_2. All solutions were sparged with N_2 for a minimum of 30 minutes prior to use.

Particles were formed using a room temperature co-precipitation technique. Iron(II) sulphate and iron(III) sulphate were dissolved in N_2 sparged MilliQ (20 mL), under an inert atmosphere of N_2 to form a 1 mM Fe solution in a two-necked round bottom flask (quantities of iron(II) sulphate and iron(III) sulphate were calculated relative to the desired Fe^{3+}/Fe^{2+} ratio). A set amount of TEPA was calculated relative to the iron content, added to the reaction mixture, and left to stir to ensure dissolution of TEPA and iron salts. N_2 sparged 0.5 M NaOH (8 mL) was added at a rate of 50 μL a minute with magnetic stirring,

for a total of 160 minutes using a Harvard Apparatus 11 plus syringe pump driver.

A schematic of the reaction set-up is shown in ESI† Fig. S10.

The reaction was then left to age for an hour under the inert atmosphere with stirring maintained. The reaction mixture was then magnetically separated, washed 5 times with sparged MilliQ to remove any non-magnetic iron oxides and NaOH, and the particles dried in a vacuum oven at 40 °C overnight. The particles were then ground with a pestle and mortar for analysis.

Magnetite nanoparticle characterisation

Transmission Electron Microscopy (TEM). For TEM analysis of magnetic nanoparticles, a 10 μL of a 1 mg mL^{-1} suspension of nanoparticles was sonicated for 1 minute in hexane and dropped onto a carbon coated copper TEM grid and allowed to dry down for a minimum of 1 hour. Grids were imaged using a FEI Tecnai G2 Spirit electron microscope (Thermo Scientific, Waltham, MA, United States) and the TEM images were analysed using Image-J software (v1.52, public domain, National Institute of Health, MD, USA). >200 particles per sample were randomly selected for measurement. Further details on the shape and size analysis from TEM images can be found in the ESI.†

Vibrating Sample Magnetometry (VSM). Magnetic susceptibility was performed on a known quantity (1–5 mg) of dry iron oxide nanoparticles on a MPMS 3 SQUID magnetometer (Quantum Design, Surrey, United Kingdom) in vibrating sample mode, with the samples packed in size 3 gelatine capsules. The samples were run at 300 K between −3 and 3 T with a sweep rate of 0.01 T s^{-1}. The data shown is cropped at saturation magnetisation.

X-Ray Diffraction (XRD). For XRD data of samples was collected by analysis of dry iron oxide nanoparticles in a Bruker D8 powder diffractometer (Bruker, Coventry, United Kingdom). Diffraction images were collected at 0.022-degree increments from 20–80 degrees, with a fixed wavelength at λ = 1.54178 Å at 1.2 seconds per step from a Cu Kα X-ray source.

Factorial design

Initially, a 2^3 FFD with a centre point was utilised (data shown in ESI†). The preliminary study identified the time point of additive addition to be insignificant for the MNP properties, hence this factor was removed from future experiments. Thus, we proceeded with a 2^2 full factorial design with center point to investigate the Fe/additive ratio (factor x_1) between the boundaries 50–500 mol mol^{-1}, and the Fe^{3+}/Fe^{2+} ratio (factor x_2) between 0.2–0.6 mol mol^{-1}, as identified suitable from the literature review above, and tabulated in Table 1. The use of coded variables, essentially rescaling the x inputs between −1 and +1, has found merit for its orthogonality and is applied here where appropriate. eqn (1) and (2) were used to convert between coded and uncoded variables (see Table 1) for the Fe/additive (x_1) and Fe^{3+}/Fe^{2+} (x_2) factors respectively:

$$x_{1,\text{coded}} = \frac{x_{1,\text{uncoded}} - 275}{225} \quad (1)$$

$$x_{2,\text{coded}} = \frac{x_{2,\text{uncoded}} - 0.4}{0.2} \quad (2)$$

Based on the factorial design, first-order linear regression models were constructed for visualisation and response optimisation purposes according to eqn (3):

$$y = \beta_0 + \sum \beta_i x_i + \sum \beta_{ij} x_i x_j \quad (3)$$

where y is the response, β_0 is the average, β_i are the regression coefficients of the main factors, β_{ij} are the regression coefficients of the factor interactions, and x_i and x_j are the regressor variables of the factors or factor interactions.

Path of Steepest Ascent (PSA)

Using the first-order model established during the screening experiment (eqn (3)), the path of steepest ascent was evaluated for each response from:

$$\nabla y\Big|_{(0,0)} = \frac{\partial}{\partial x_i}\left(\beta_0 + \sum \beta_i x_i + \sum \beta_{ij} x_i x_j\right)\Big|_{(0,0)}, \quad \frac{\partial}{\partial_{xj}}\left(\beta_0 + \sum \beta_i x_i + \sum \beta_{ij} x_i x_j\right)|_{(0,0)} \quad (4)$$

Table 1 Input parameters and experimental results of the factorial design. Experiments were carried out as duplicates

Factors				Responses[a]	
Fe/additive ratio, x_1 (mol mol^{-1})		Fe^{3+}/Fe^{2+} ratio, x_2 (mol mol^{-1})			
Coded	Uncoded	Coded	Uncoded	Shape (% isotropically faceted)	Saturation magnetisation (emu g^{-1})
−1	50	−1	0.2	39, 41	41.7, 69.1
+1	500	−1	0.2	58, 54	31.3, 38.3
−1	50	+1	0.6	87, 92	75.7, 78.0
+1	500	+1	0.6	11, 13	66.9, 74.2
0	275	0	0.4	14, 18	59.2, 78.0

[a] Results represent values from duplicate experiments (separated by a comma).

where ∂ are partial derivatives evaluated at (0,0), resulting in a straight line with the origin at the center point of the factorial design. Because the paths of steepest ascent for the shape and magnetisation responses diverged in different directions, an optimised line between the two was taken as the final PSA in an endeavour to optimise both responses simultaneously. The PSA was then divided into five equal segments between the center point and the physical limits of MNP synthesis of Fe/additive ≥ 5.0 and Fe^{3+}/Fe^{2+} ≤ 0.64, resulting in six steps (Table 2).

Results

Response consideration

When considering the quality of particles desired for biomedical applications, two key responses of potential optimisation were identified: i) the percentage of faceted particles, and ii) the saturation magnetisation. As elongated nanorods have been previously found to exhibit cytotoxic effects,[48] the focus was kept on isotropic (equal size along each axis) faceted particles. Due to the nature of TEM imaging returning a two-dimensional image, particle shapes are assigned by the presence of defined facets (Fig. S13, ESI†) with a large number (>300) of particles being inspected for shape analysis. Saturation magnetisation is highly indicative of the magnetic purity of particles formed, with pure magnetite exhibiting a saturation magnetisation of 92 emu g^{-1}. High magnetic saturation is desired for industrial applications.

An initial scouting experiment found the time point of additive addition to be an insignificant factor in both the shape and magnetism responses of MNP and was hence deleted from further experiments (see ESI†).

The two remaining factors Fe/additive ratio and Fe^{3+}/Fe^{2+} ratio were used to simultaneously optimise the shape (% isotropic faceted particles) and saturation magnetisation (emu g^{-1}) responses by employment of a factorial designed followed by a path of steepest ascent optimisation.

Factorial design

Table 1 tabulates the experimental results for the factorial design. For each response, a first-order linear regression model was constructed according to eqn (3) with the Minitab 19 Software[49] (Table 3). Analysis of variance (ANOVA) was performed to evaluate the adequacy and predictability of the models (also Table 3), as well as to segregate significant from insignificant factors with a level of significance of $\alpha = 0.05$.

The ANOVA shows several key findings; i) Fe/additive ratio is significant for the shape response, but not magnetism, ii) Fe^{3+}/Fe^{2+} is significant for magnetism but not shape, iii) the interaction of Fe/additive ratio and Fe^{3+}/Fe^{2+} is significant for shape but not magnetism.

Previously conducted research has shown the importance of additive concentration on the proportion of faceted particles, with a higher % of particles appearing faceted as the Fe/additive ratio increases.[23] As more additive is present, a greater inhibition of growth may occur on developing crystal facets, resulting in an increased proportion of shape-controlled particles. This is shown in Fig. 2, with the proportion of isotropic faceted particles being highest at a 1 : 50 Fe/additive ratio and 0.6 ferric ratio (87 and 92% faceted for the two repeats). This improved morphology is not observed at the equivalent 1 : 500 Fe/additive ratio, instead producing the lowest proportion of isotropic faceted particles (11 and 13%).

As the interaction between Fe/additive ratio and Fe^{3+}/Fe^{2+} was found to be significant for shape, this synergy results in the effect of one factor being dependent on the level of the other factor. This means that because a consistent Fe/additive ratio fails to produce identical results at different ferric ratios, the shape depends on the levels of both factors, which is termed an interaction. Thus, the shape is influenced by a coupled effect between both the Fe/additive and Fe^{3+}/Fe^{2+} ratio.

The addition of higher concentrations of additive were not found to significantly influence saturation magnetisation within these experimental parameters.

The key influencing factor for particle magnetism was found to be Fe^{3+}/Fe^{2+}. This ratio is responsible for the iron oxides formed, with magnetite formation being favoured at the optimal 2 : 1 ratio. At lower ferric ratios ferrous-rich non-magnetic iron oxides are formed, leading to a product of mixed iron oxides containing non-magnetic iron oxides, and reduced saturation magnetisation.

When the path of steepest ascent is constructed mathematically, higher-order terms are neglected, making

Table 2 Treatment steps and experimental results along the path of steepest ascent. Experiments were carried out as duplicates

	Factors				Responses[a]	
	Fe/additive ratio, x_1 (mol mol^{-1})		Fe^{3+}/Fe^{2+} ratio, x_2 (mol mol^{-1})			
Step	Coded	Uncoded	Coded	Uncoded	Shape (% isotropically faceted)	Saturation magnetisation (emu g^{-1})
0	0	275	0	0.40	19, 17	62.8.3, 61.6
1	−0.24	221	0.24	0.45	26, 31	67.8, 73.4
2	−0.48	167	0.47	0.49	20, 25	86.4, 90.6
3	−0.72	113	0.71	0.54	16, 16	91.1, 84.5
4	−0.96	59	0.95	0.59	96, 94	67.7, 63.0
5	−1.2	5	1.19	0.64	45, 54	67.4, 76.8

[a] Results represent values from duplicate experiments (separated by a comma).

Table 3 Regression models and analysis of variance for the shape and magnetisation response based on a confidence interval of 95%

	Shape (% isotropic faceted particles)					Saturation magnetisation (emu g^{-1})				
Uncoded[a]	$y = 1.3 + 0.14x_1 + 150x_2 - 0.52x_1x_2$					$y = 49.5 - 0.0615x_1 + 49.8x_2 + 0.0792x_1x_2$				
Coded[b]	$y = 42.51 - 15.34x_1 + 1.39x_2 - 23.4x_1x_2$					$y = 61.24 - 6.71x_1 + 14.31x_2 + 3.57x_1x_2$				
Source	DF[c]	SS[d]	MS[e]	F-Value[f]	p-Value[g]	DF[c]	SS[d]	MS[e]	F-Value[f]	p-Value[g]
Fe/additive	1	1882	1882	6.34	0.045[n]	1	360	360	2.91	0.139
Fe^{3+}/Fe^{2+}	1	15	15	0.05	0.827	1	1638	1638	13.27	0.011[n]
Fe/additive × Fe^{3+}/Fe^{2+}	1	4382	4382	14.75	0.009[n]	1	101.7	101.7	0.82	0.339
Residual[h]	6	1782	297			6	741	123		
Curvature[i]	1	1750	1750	270.83	0.000	1	135	135	1.11	0.34
Pure error[j]	5	32	6			5	606	121		
Total	9	8062				9	2840			
$R^{2,k}$	0.78					0.74				
Adjusted $R^{2,l}$	0.67					0.61				
Prediction $R^{2,m}$	0.62					0.29				

[a] Model with factors in original units of mol mol^{-1}. [b] Model with factors rescaled between −1 and +1. [c] Degrees of Freedom (DF). [d] Sum of squares (SS). [e] Mean square (MS). [f] The MS of a factor divided by the residual MS. [g] Source is statistically significant if p-value $< \alpha$ (0.05). [h] Error. [i] Presence of significant interaction terms causing bending or curvature of the response surface. [j] Residual or error calculated from replicated observations. [k] Coefficient of multiple determination. [l] R^2 accounting for statistically significant terms in the model. [m] R^2 evaluating the predictability of a missing observation. [n] Statistically significant factor or interaction.

complex models redundant at an early stage of optimisation. Nevertheless, the ANOVA shows that curvature is significant for the shape of MNP, suggesting that a model based on main effects only is inappropriate to explain the trend fully. According to the non-hierarchy principle, it is indeed possible for a factor to be insignificant on its own but to be part of a large interaction.[50,51] On the other hand, the insignificance of curvature for magnetism could suggest that a simple model is sufficient in this case. However, significant deviation from the predictions of the model was observed, making the PSA optimisation beyond the original design promising.

The R^2 values of 0.78 and 0.74 for shape and magnetism respectively indicate that 78 and 74% of the trend in shape and magnetism can be explained by the model. Moreover, most types of R^2 statistics were above 0.6, giving confidence in the models for development of the consecutive PSA.

Fig. 3 shows three-dimensional (3D) response surfaces and contour plots of the regression models for the shape and magnetisation respectively. A contour plot is essentially a top-down view of the 3D model, in which lines of constant response are drawn.

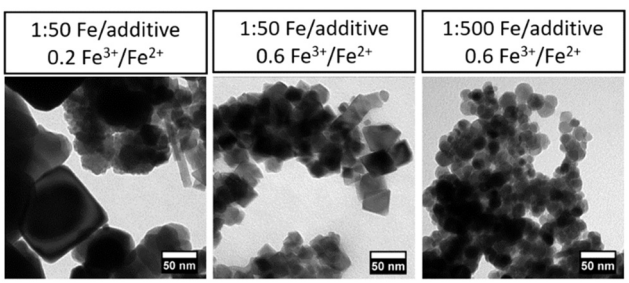

Fig. 2 Representative TEM images of particles formed under stated conditions in the factorial design of magnetite synthesis with TEPA additive.

Path of steepest ascent

As the preceding factorial design did not identify a maximum response, the search for optimum synthesis conditions is required to move beyond the initial design in the most efficient direction, which is generally assumed to be the direction in which the responses increase steepest.[52]

Using coded regression models (Table 3), individual paths of steepest ascent were calculated for the shape and saturation magnetisation respectively in coded units:

$$x_2 = -0.0906x_1 \quad (5)$$

$$x_2 = -2.1326x_1 \quad (6)$$

From comparison of eqn (5) and (6), and likewise from the responses shown in Fig. 3, it was observed that the shape and magnetism responses increased in differing directions. In pursuit of the best compromise between the two responses, an optimised PSA was constructed with equation $x_2 = -1.0108x_1$ dividing the sector between the two individual PSAs in two.

This optimised path was then divided into 6 steps between the midpoint (Fe/additive = 275 mol mol^{-1}, Fe^{3+}/Fe^{2+} = 0.4 mol mol^{-1}) and the physical limits of MNP synthesis (Fe/additive ≥ 5.0 and $Fe^{3+}/Fe^{2+} \leq 0.8$), resulting in the PSA extending beyond the initial factorial design shown in the contour plot in Fig. 4 with the steps illustrated in red.

The coded variables were converted to uncoded ones according to eqn (1) and (2) and are tabulated alongside the experimental results in Table 2.

For the shape and magnetism responses respectively, Fig. 5 shows the actual results and the values predicted by the first-order models along the optimised PSA. The discrepancies between predicted and actual values reinforce

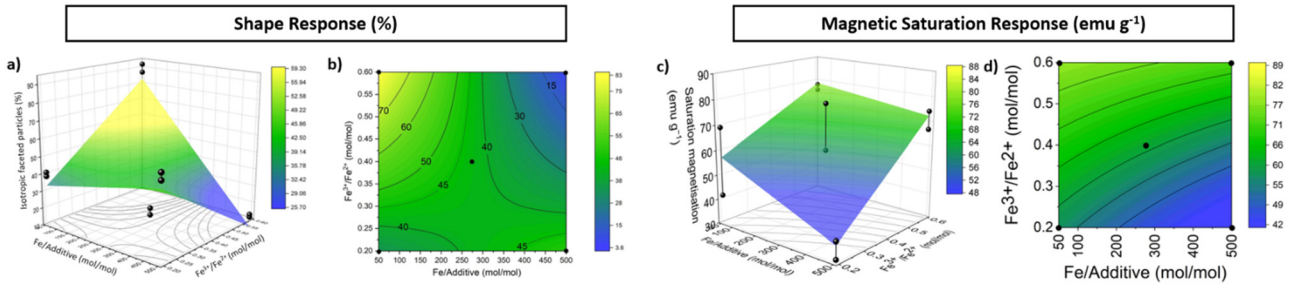

Fig. 3 Three-dimensional response surfaces for a) the shape and c) the magnetism response, and contour plots for b) the shape and d) the magnetism response, each based on the first-order regression models from the FFD.

the fact that factorial designs may indicate the direction of a global maximum, but a sequential strategy is required to identify its precise location and local minima or maxima in its vicinity.

The maximum % isotropic faceted particles occurred with 95% (average of both experimental values) at the fourth step, and the maximum saturation magnetisation occurred at the third step with 88.5 emu g^{-1}.

Discussion

The co-precipitation of magnetite from solution is a complex reaction, which proceeds through a series of intermediary ferric and ferrous based iron oxides to form magnetite.[53] As such, the experimental landscape may not be straightforward, and different levels of factors interacting may considerably alter the morphology and magnetism of particles formed in a non-linear manner. Many co-precipitation particle syntheses consider mild oxidation to obtain the final magnetite product, hence syntheses with Fe^{3+}/Fe^{2+} ratios of >0.66 are still successful at producing magnetic particles despite an excess of ferrous ions.

The process of iterative DoE has taken steps toward mapping said experimental landscape, with several experimental conditions being identified as points of interest for further study which will be discussed below.

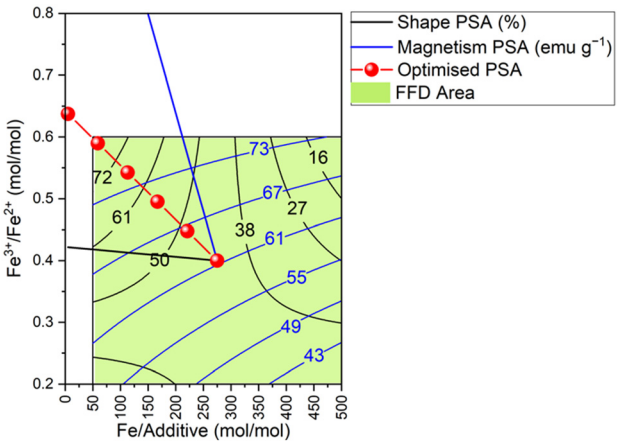

Fig. 4 Contour plot depicting direction of increasing response for the shape (black) and magnetism response (blue), leading to the optimised path of steepest ascent (red) with 6 steps.

From the first scouting FFD the time point of additive addition was found to be an insignificant factor. This suggests the function of TEPA as an additive under these conditions was to interact with forming magnetite surfaces, influencing particle growth *via* inhibition of facet growth rather than *via* interaction with aqueous iron ions. This is concurrent with molecular dynamics simulations suggesting TEPA has an exothermic binding energy at the [111] octahedral magnetite surface.[23] Deletion of the time variable also allowed for future designs to be simplified, as the addition of TEPA at the beginning of the reaction did not appear to impair the formation of the desired product.

The first FFD also considered size as a response, with size being influenced significantly by both the Fe^{3+}/Fe^{2+} and Fe/additive ratios. Higher concentrations of TEPA led to a reduction in particle size at a low ferric ratio (0.2), producing particles in accordance (closer to 20 nm) with those produced at a more ideal ferric ratio (0.6). The ferric ratio has previously been found to drastically influence the size of particles formed, with particles formed at higher ratios (0.5–0.7) being significantly smaller in size than those formed at lower ratios (0.2–0.4). This was seen alongside a significant increase in saturation magnetisation suggesting that as well as particle size decreasing, the addition of TEPA also promoted the formation of greater proportions of magnetite at sub-optimal Fe^{3+}/Fe^{2+} ratios. As the experiments progressed through further iterations it was decided to focus on shape tuning and optimising magnetic response to simplify the designs and streamline optimisation.

The second FFD identified the Fe/additive ratio as significant for the proportion of isotropic faceted particles formed, with Fig. 3 exemplifying the difference in particles formed at the same Fe^{3+}/Fe^{2+} ratio with varied Fe/additive ratio. This increase in proportion of isotropic faceted particles is likely due to the larger quantity of additive having an increased inhibition effect on specific facet growth. A concentration study has been previously conducted which found a Fe/additive ratio of 125 : 1 was preferred to a lower iron concentration of 12.5 : 1.[23] This study tested an intermediate value of 50 : 1 between the previously explored experimental values, which was found to produce highly

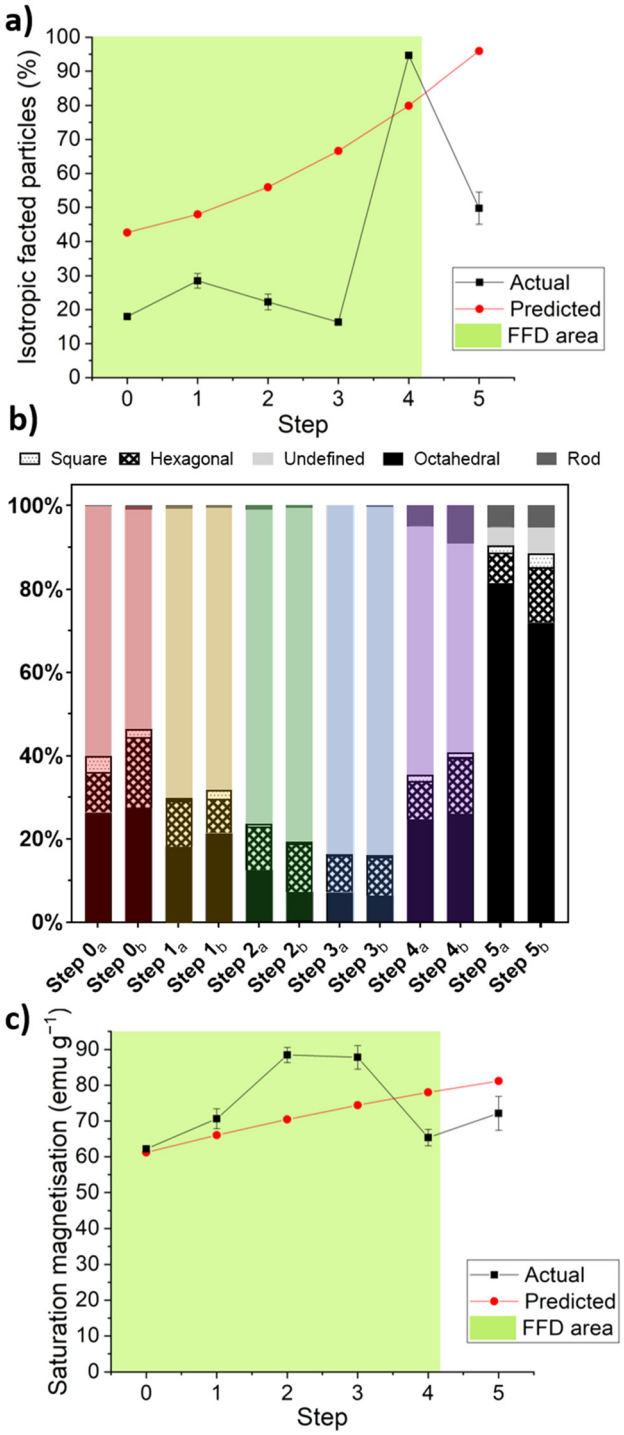

Fig. 5 Actual results and values predicted by the optimised PSA for a) the shape; b) shape frequency graph of particles; and c) the saturation magnetisation responses. Error bars are range of duplicate experiments.

optimal particles (~90% faceted and 80.9 emu g^{-1}). Notably, these particles are the best compromise between performance of both the shape and magnetic response and are hence deemed as the preferred conditions for further investigation into the effect of TEPA as an additive on magnetite co-precipitations. As the PSA varied two factors simultaneously, it is not possible to draw parallels between all points of the previous concentration study due to the effect of also varying the Fe^{3+}/Fe^{2+} ratio simultaneously, and the resultant effect this may have on the proportion of faceted particles formed.

Fig. 3 also draws a contrast to the effect of the lower (0.2) Fe^{3+}/Fe^{2+} ratio on particles formed. Whilst particle size is not analysed as a response in these designs, the particles are visibly less consistent with reduced magnetism relative to the particles formed at a 0.6 ratio. This reduction in saturation magnetisation can occur due to the formation of other non-magnetic iron oxides being favoured the further from the ideal ratio of 2 : 1 Fe^{3+}/Fe^{2+} ions. This is supported by XRD data (Fig. 6) showing that the XRD of particles formed at a low ferric ratio with a low concentration of additive exhibited a ferrous rich green rust and wüstite impurity peaks. These peaks were not observed in the sample formed at the same low ferric ratio with a higher Fe/additive ratio, supporting the theory that at highly sub-optimal ratios, high concentrations of TEPA may be aiding the formation of magnetite.

Interestingly, a lower Fe^{3+}/Fe^{2+} ratio can lead to more faceted particles. This effect can occur for two reasons: i) when a particle is larger in size their facets have had longer to grow and mature compared to smaller particles, and ii) not all particles present at lower ferric ratios will be magnetite. The presence of iron oxide impurities with different morphologies may explain the greater proportion of faceted particles forming at the lower ferric ratio compared to the particles synthesised at a 0.6 ratio with 50 : 1 additive ratio. A similar pattern has been observed prior with the formation of hexagonal plates of green rust, which is also observed in the XRD of the 0.2 Fe^{3+}/Fe^{2+} 500 : 1 Fe/additive ratio reaction.[54]

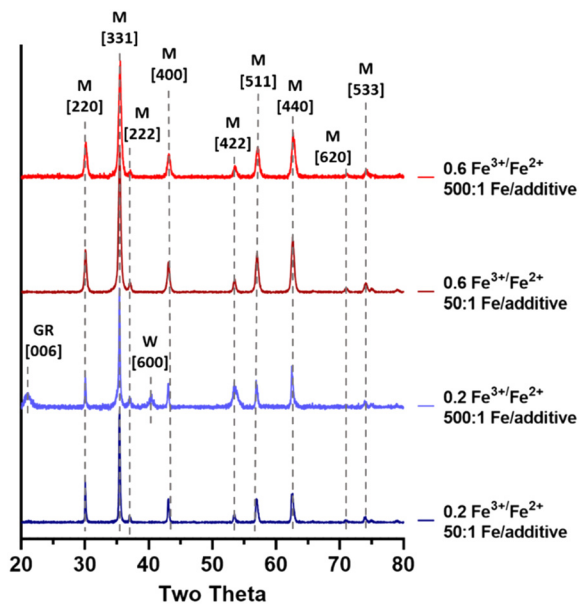

Fig. 6 Annotated XRD data for magnetic particles formed with high and low levels of Fe^{3+}/Fe^{2+} ratio and Fe/additive ratio, where M = magnetite, GR = green rust, and W = wüstite.

In contrast to the considerable change observed in shape response with the Fe/additive ratio, saturation magnetisation was not found to be significantly influenced by a change in Fe/additive ratio. This suggests in contrast with the first design that TEPA is neither promoting the formation of higher quality magnetite, nor lowering the particle quality, which can occur when an additive is embedded in the forming nanoparticle structure lowering the overall particle crystallinity. As the first FFD included Fe^{3+}/Fe^{2+} ratios further from the 2 : 1 stoichiometric ratio of ferrous and ferric ions natively found within magnetite, it is possible the improved magnetic response is only observed at ratios very far from the ideal. Any assumption made cannot be extrapolated to all concentrations of additive and can only be considered the case for the conditions tested within the experimental design, as the effects of higher proportions of additive were found to lower particle magnetism in the PSA.

The particles formed at a 0.6 Fe^{3+}/Fe^{2+} ratio and 50 : 1 Fe/additive ratio were significantly more faceted than those formed under any of the other conditions, highlighting the interaction between the two factors. TEPA is less effective at tuning the shape of particles formed at lower Fe^{3+}/Fe^{2+} ratios, perhaps due to the formation of other iron oxides. The higher Fe/additive ratio produced less faceted particles than the lower ratio at the 0.2 Fe^{3+}/Fe^{2+} ratio possibly due to the previously mentioned effect of an increased TEPA concentration producing smaller particles which are often generally less faceted at lower ferric ratios.

The PSA design successfully identified a maximum for both the shape and magnetic response, albeit not at the same step. While it is difficult to maximise both responses simultaneously, as the individual maxima occur at different steps (shape maximum at step 4, magnetism maximum at step 3), it is still possible to evaluate an optimum operating range between both responses. A midpoint between step 3 and 4 is likely to offer the best agreement, predicted to produce 75% isotropic faceted particles with 75 emu g^{-1} saturation magnetisation.

Consistent with prior research,[23] Fe/additive ratios appear to have a peak concentration at which they are most effective, above which there are diminishing returns. Above this concentration the additional TEPA may act to alter the pH of the reaction in a manner which is unfavourable.

This diminishing returns effect also appears in the magnetic data, with magnetism generally increasing until step 3, at which point it drops. When comparing the second FFD with the PSA, it was found that similar conditions (FFD – Fe/additive: 50 : 1, Fe^{3+}/Fe^{2+}: 0.6) (PSA – Fe/additive: 59 : 1, Fe^{3+}/Fe^{2+}: 0.59) produced particles with lower magnetism of 65.4 emu g^{-1} (FFD) compared to 76.9 emu g^{-1} (PSA). The sensitive nature of co-precipitations may have led to a small less controllable change in conditions (room temperature, humidity, *etc.*) forming less magnetic particles.

Several data points within the second FFD and PSA show a discrepancy in magnetic data (Tables 1 and 2) with one repeat producing more highly magnetic particles. For future work, further control over these discrepancies may be prudent. A magnetic reading of >60 is still deemed highly magnetic, with one laboratory using superparamagnetic particles with a saturation magnetisation of 25–35 emu g^{-1} (BioMag©),[55] hence suggesting the particles synthesised in these designs would be sufficiently magnetic for biomedical use.

From the experimental conditions covered in the three designs, the optimal particles were produced at a 0.6 Fe^{3+}/Fe^{2+} ratio and 50 : 1 Fe/additive ratio. Whilst the PSA did not reveal an improvement in particle properties over the second FFD, it is important to push the boundaries of experimental design in the search for optimal MNP synthesis in the event ideal conditions are outside the previously tested ranges.

Conclusions

DoE has been utilised through three iterations of experiments to investigate the previously unexplored reaction landscape of additive addition to MNP co-precipitation. By seeking to optimise the shape and magnetic response simultaneously through a combination of FFD and PSA, several findings have been identified.

The time-point of TEPA addition was not found to play a significant role, suggesting it can be added to the reaction at a later point if required without detrimental effect to particle quality. This allows for the potential of future synthesis to be simplified, whilst further building on our understanding of how TEPA functions as an additive.

The upper and lower limitations of high quality isotropic faceted MNP synthesis have been explored, with reduced magnetism observed at lower Fe^{3+}/Fe^{2+} ratios, showcasing the importance of a close to 2 : 1 stoichiometric ratio, with a ratio of 0.6 generally producing the particles with the highest magnetic properties. Optimal isotropic faceted particle formation was observed at 59 : 1 and 50 : 1 Fe/additive ratios, at 0.59/0.6 Fe^{3+}/Fe^{2+} ratios respectively, further highlighting the importance of a ferric ratio close to 0.6.

This work is a compelling step on the pathway to statistically guided and tuneable MNP synthesis, with the shape control of MNP having not yet being extensively researched under RTCP conditions. By building upon the prior studies of the influence of TEPA in the co-precipitation system, we have furthered our understanding of how additive concentration and ferric ratio influence the properties of MNP formed and identified a potential starting point for batch scale-up of isotropic faceted MNP.

Abbreviations

3D	Three-dimensional
ANOVA	Analysis of variance
DF	Degrees of freedom
DoE	Design of Experiments
FFD	Full factorial design
MIA	Magnetite interacting adhiron
MNP	Magnetite nanoparticles

MS	Mean square
OFAT	One-factor-at-a-time
RTCP	Room temperature co-precipitation
SS	Sum of squares
TEM	Transmission electron microscopy
TEPA	Tetraethylenepentamine
VSM	Vibrating sample magnetometry
XRD	X-Ray diffraction

Conflicts of interest

There are no conflicts to declare.

Acknowledgements

This work was supported by funding from the EPSRC (grant number EP/P006892/1) and the University of Sheffield's EPSRC DTP allowance (grant number EP/M508135/1) funds Laura Norfolk's PhD. We thank S. Tsokov, C. Hill (Sheffield Electron Microscopy unit) for TEM training, Nicola Morley and Zhao Leong for VSM training, Heather Grieveson for ICP measurements, and Craig Robertson for support with powder XRD.

References

1 A. E. Rawlings, L. A. Somner, M. Fitzpatrick-Milton, T. P. Roebuck, C. Gwyn, P. Liravi, V. Seville, T. J. Neal, O. O. Mykhaylyk, S. A. Baldwin and S. S. Staniland, *Nat. Commun.*, 2019, **10**, 1–9.
2 S. M. Bird, A. E. Rawlings, J. M. Galloway and S. S. Staniland, *RSC Adv.*, 2016, **6**, 7356–7363.
3 R. E. Rosensweig, *Sci. Am.*, 1982, 136–145.
4 D. Yuvarajan and M. V. Ramanan, *Arabian J. Sci. Eng.*, 2016, **41**, 2023–2030.
5 K. Mahmoudi, A. Bouras, D. Bozec, R. Ivkov and C. Hadjipanayis, *Int. J. Hyperthermia*, 2018, 1–13.
6 Q. A. Pankhurst, J. Connolly, S. K. Jones and J. Dobson, *J. Phys. D: Appl. Phys.*, 2003, **36**, 167–181.
7 R. Weissleder, D. D. Stark, B. L. Engelstad, B. A. Bacon, D. L. White, P. Jacobs and J. Lewis, *Am. J. Roentgenol.*, 1989, **152**, 167–173.
8 M. Wahajuddin and S. Arora, *Int. J. Nanomed.*, 2012, **7**, 3445–3471.
9 A. E. Rawlings, J. P. Bramble, A. A. S. Tang, L. A. Somner, A. E. Monnington, D. J. Cooke, M. J. McPherson, D. C. Tomlinson and S. S. Staniland, *Chem. Sci.*, 2015, **6**, 5586–5594.
10 A. G. Roca, L. Gutiérrez, H. Gavilán, M. E. Fortes Brollo, S. Veintemillas-Verdaguer and M. del P. Morales, *Adv. Drug Delivery Rev.*, 2019, **138**, 68–104.
11 J. Mohapatra, A. Mitra, M. Aslam and D. Bahadur, *IEEE Trans. Magn.*, 2015, **51**, 3–6.
12 S. V. Patwardhan, J. R. H. Manning and M. Chiacchia, *Curr. Opin. Green Sustainable Chem.*, 2018, **12**, 110–116.
13 D. Maity, S. N. Kale, R. Kaul-Ghanekar, J. M. Xue and J. Ding, *J. Magn. Magn. Mater.*, 2009, **321**, 3093–3098.
14 M. Unni, A. M. Uhl, S. Savliwala, B. H. Savitzky, R. Dhavalikar, N. Garraud, D. P. Arnold, L. F. Kourkoutis, J. S. Andrew and C. Rinaldi, *ACS Nano*, 2017, **11**, 2284–2303.
15 S. V. Patwardhan and S. S. Staniland, *Green Nanomaterials*, 2019.
16 A. E. Rawlings, J. P. Bramble, A. M. Hounslow, M. P. Williamson, A. E. Monnington, D. J. Cooke and S. S. Staniland, *Chem. – Eur. J.*, 2016, **22**, 7885–7894.
17 A. E. Rawlings, J. P. Bramble, R. Walker, J. Bain, J. M. Galloway and S. S. Staniland, *Proc. Natl. Acad. Sci. U. S. A.*, 2014, **111**, 16094–16099.
18 Y. Kuwahara, T. Miyazaki, Y. Shirosaki, G. Liu and M. Kawashita, *Ceram. Int.*, 2016, **42**, 6000–6004.
19 R. Blakemore, *Science*, 1975, **190**, 377–379.
20 A. Arakaki, J. Webb and T. Matsunaga, *J. Biol. Chem.*, 2003, **278**, 8745–8750.
21 D. Murat, V. Falahati, L. Bertinetti, R. Csencsits, A. Körnig, K. Downing, D. Faivre and A. Komeili, *Mol. Microbiol.*, 2012, **85**, 684–699.
22 A. E. Rawlings, J. P. Bramble, A. A. S. Tang, L. A. Somner, A. E. Monnington, D. J. Cooke, M. J. McPherson, D. C. Tomlinson and S. S. Staniland, *Chem. Sci.*, 2015, **6**, 5586–5594.
23 L. Norfolk, K. Kapusta, D. Cooke and S. Staniland, *Green Chem.*, 2021, **23**, 5724–5735.
24 R. Pilling, S. R. Coles, M. R. Knecht and S. V. Patwardhan, *Comms. Eng.*, 2023, **2**, 78.
25 L. Dewulf, M. Chiacchia, A. S. Yeardley, R. A. Milton, S. F. Brown and S. V. Patwardhan, *Mol. Syst. Des. Eng.*, 2021, **6**, 293–307.
26 A. Rodríguez-López, A. Paredes-Arroyo, J. Mojica-Gomez, C. Estrada-Arteaga, J. J. Cruz-Rivera, C. G. Elías Alfaro and R. Antaño-López, *J. Nanopart. Res.*, 2012, **14**, 1–9.
27 E. Mohammad, E. I. Reza and N. Bahram, *Asian J. Chem.*, 2008, **20**, 3857–3865.
28 T. Raut, B. Shriwastava, P. Sharma, P. Gide, G. Deokar, S. Rahane and K. Erande, *Part. Sci. Technol.*, 2016, **34**, 509–516.
29 K. Al-Saad, A. A. Issa, S. Idoudi, B. Shomar, M. A. Al-Ghouti, N. Al-Hashimi and M. El-Azazy, *Molecules*, 2020, **25**, 1–20.
30 N. C. V. Rost, F. M. Broca, G. C. Gonçalves, M. A. Cândido, M. L. Castilho and L. J. Raniero, *Braz. J. Phys.*, 2019, **49**, 22–27.
31 M. Mahmoudi, A. Simchi, M. Imani, A. S. Milani and P. Stroeve, *J. Phys. Chem. B*, 2008, **112**, 14470–14481.
32 A. González Moreno, M. M. López Guerrero, E. Vereda Alonso, A. García De Torres and J. M. C. Pavón, *New J. Chem.*, 2017, **41**, 8804–8811.
33 H. C. Roth, S. P. Schwaminger, M. Schindler, F. E. Wagner and S. Berensmeier, *J. Magn. Magn. Mater.*, 2015, **377**, 81–89.
34 N. Mizutani, T. Iwasaki and S. Watano, *Nanomater. Nanotechnol.*, 2015, **5**, 1–7.
35 D. Forge, A. Roch, S. Laurent, H. Tellez, Y. Gossuin, F. Renaux, L. Vander Elst and R. N. Muller, *J. Phys. Chem. C*, 2008, **112**, 19178–19185.
36 S. P. Schwaminger, C. Syhr and S. Berensmeier, *Crystals*, 2020, **10**, 1–12.

37 J. Medinger, M. Nedyalkova and M. Lattuada, *Nanomaterials*, 2021, **11**, 1–19.
38 G. Fan, Y. Zhu, Z. Fu, B. Sun, C. Teng, R. Yang and X. Li, *3 Biotech*, 2020, **10**, 1–15.
39 C. Li, L. Li, H. Zhou, C. Xia and L. He, *J. Braz. Chem. Soc.*, 2015, **26**, 247–254.
40 X. J. Jiang, Y. Hu, L. Jiang, B. Zou, P. Song and H. Huang, *Biotechnol. Bioprocess Eng.*, 2013, **18**, 350–357.
41 S. Zhang and J. D. Cui, *Biotechnol. Biotechnol. Equip.*, 2012, **26**, 3418–3423.
42 C. L. Yao, C. H. Liu, I. M. Chu, T. B. Hsieh and S. M. Hwang, *Enzyme Microb. Technol.*, 2003, **33**, 343–352.
43 E. R. El-Helow and A. M. El-Ahawany, *Enzyme Microb. Technol.*, 1999, **24**, 325–331.
44 C. Jiang, G. Sun, Z. Zhou, Z. Bao, X. Lang, J. Pang, Q. Sun, Y. Li, X. Zhang, C. Feng and X. Chen, *Int. J. Biol. Macromol.*, 2019, **121**, 293–300.
45 C. Pizarro, M. A. Fernández-Torroba, C. Benito and J. M. González-Sáiz, *Biotechnol. Bioeng.*, 1997, **53**, 497–506.
46 Y.-C. Hsiao and C.-C. Hu, *J. Electrochem. Soc.*, 2013, **160**, H279–H284.
47 B. Ghosh, D. C. Agrawal and S. Bhatia, *Ind. Eng. Chem. Res.*, 1994, **33**, 2107–2110.
48 N. Doshi and S. Mitragotri, *J. R. Soc., Interface*, 2010, **7**, 1–8.
49 *Minitab (v19)*, Minitab LLC, Pine Hall, PA, 2020.
50 D. C. Montgomery, R. H. Myers, W. H. Carter and G. G. Vining, *Qual. Reliab. Eng. Int.*, 2005, **21**, 197–201.
51 B. E. Ankenman and A. M. Dean, *Handbook of Statistics*, 2003, vol. 22, pp. 263–317.
52 D. C. Montgomery, *Design and Analysis of Experiments*, Wiley, Hoboken, NJ, 8th edn, 2012.
53 A. E. Rawlings, J. P. Bramble, A. M. Hounslow, M. P. Williamson, A. E. Monnington, D. J. Cooke and S. S. Staniland, *Chem. – Eur. J.*, 2016, **22**, 7885–7894.
54 L. Norfolk, A. E. Rawlings, J. P. Bramble, K. Ward, N. Francis, R. Waller, A. Bailey and S. S. Staniland, *Nanomaterials*, 2019, **9**, 1792.
55 B. L. Inc, Magnetic Properties of Magnetic Particles, **https://www.bangslabs.com**, (accessed December 2023).